Application of the polarization model to the study of phosphoric acid media

Frank H. Stillinger and Thomas A. Weber

Bell Laboratories, Murray Hill, New Jersey 07974

Carl W. David

Department of Chemistry, University of Connecticut, Storrs, Connecticut 06268
(Received 20 October 1981; accepted 9 December 1981)

The polarization model, previously introduced to approximate both intramolecular and intermolecular interactions in water, has been extended to include pentavalent phosphorus. The extension appears to be successful in representing structures of simple compounds of P^{5+} with O^{2-} and H^+. The model has been applied to statistical mechanical study of liquid phospheric acid at 200 C, using the Monte Carlo method of computer simulation for 216-atom systems. Two versions of the simulation have been implemented corresponding to stoichiometrically equivalent but experimentally distinguishable materials: (a) 27 orthophosphoric acid molecules, and (b) a mixture of water and polyphosphoric acid. Pair correlation functions for all types of atom pairs, as well as details of acid dissociation statistics, have been computed for both materials.

I. INTRODUCTION

In the overwhelming majority of chemical applications, liquid media consist of polyatomic substances. A realistic description of these materials at the molecular level demands consideration of vibrational and conformational motions, and of deformations that can lead to dissociation reactions. Furthermore, great interest attaches to their dielectric behavior, particularly in their role as solvents for ions.

The "polarization model"[1-3] was recently introduced to provide statistical mechanics with a convenient theoretical format in which these attributes might quantitatively be described. This model postulates a specific class of nonadditive interactions acting between atoms in preassigned oxidation states. The resulting overall potential energy algorithm (a) causes the requisite molecular species spontaneously to form, (b) automatically generates both intramolecular and intermolecular force fields, and (c) permits dissociative and exchange chemical reactions to occur. Quantitative applications have been undertaken for H_2O,[1,4,5] for HF,[2,6] and for NH_3.[7]

The present paper extends the polarization model to a chemically much more complicated case, namely the $P_2O_5 + H_2O$ system. Because the various functions employed in the model are transferrable, the previously considered pure water system becomes a starting point, and we need simply to provide for the additional presence of pentavalent phosphorous ions.

The single new bond function ϕ_{PO} required for the extension is established in Sec. II. Stable structures (according to the polarization model) for several small phosphorous-containing molecules are then reported in Sec. III. To the extent that comparisons with experiment are possible, these results seem to indicate that the polarization model can successfully represent the complex structural chemistry involved. Therefore, we have proceeded to apply the polarization model to examination of condensed phases of phosphoric acid. For this task, we have employed the Monte Carlo method of simulation, with details presented in Sec. IV.

The Monte Carlo computation has been carried out in two versions that differ in the patterns of chemical bonds present, though both share the same atomic stoichiometry. The first of these (Sec. V) consists of separate and distinct orthophosphoric acid molecules H_3PO_4. The second (Sec. VI) involves a mixture of polyphosphoric acid molecules with water and orthophosphoric acid. Since the time scale over which phosphate–phosphate linkages hydrate in the latter far exceeds that of the computation, these two cases have been treated as representing distinguishable substances. This accords with slow hydrolysis rates observed experimentally.[8]

Our decision to investigate the phosphoric acid system was based on potential importance of results obtained for several fields. First, polyphosphoric acid is occasionally employed as a reaction medium for certain organic syntheses.[9] Second, phosphoric acid has become an important high-temperature electrolyte for use in fuel cells.[10] Third, the opportunity eventually to observe and describe the hydration process for phosphate linkages at the molecular level may offer some insight into the analogous biochemistry of the ATP → ADP degradation.[11] The present work should be viewed as an exploratory prerequisite for later, more detailed, studies aimed at contributing to each of these areas.

II. EXTENSION TO PHOSPHOROUS

In the general polarization model context, the overall potential energy Φ for a collection of atomic species is postulated to consist of two parts,

$$\Phi = \Phi_{pair} + \Phi_{pol} \ . \qquad (2.1)$$

The first is a sum of central pair potentials for all pairs of particles present. The second is a many-body polarization energy that generalizes the corresponding expression for charged and polarizable points in classical electrostatics.

In the case of pure water two types of particles are present. These are taken to be O^{2-} and H^+. The former

 0021-9606/82/063131-13$02.10

is polarizable; the latter (bare proton) has vanishing polarizability. Appendix A provides full details concerning the general structure of Φ and the specific functions employed for O^{2-} and H^{+}.

We now wish to add pentavalent phosphorous P^{5+} to the collection of available particles. On account of its high positive charge, we have felt justified in neglecting polarizability for this species. Hence, each of these new particles will be treated just as point charges analogous to H^{+}. The immediate consequence is that pair interactions for two phosphorous particles or for a phosphorous and a hydrogen have elementary Coulombic form

$$\phi_{PP}(r) = 25\,e^2/r\,, \qquad \phi_{PH}(r) = 5\,e^2/r\,. \tag{2.2}$$

The only really new ingredient required is the pair function $\phi_{PO}(r)$. Due to the charges assigned to phosphorous and oxygen, the large-r limiting form is obvious:

$$\phi_{PO}(r) \sim -10e^2/r\,. \tag{2.3}$$

But at small distances, deviations from this form must occur as the phosphorous penetrates the spatially extended electron cloud of the oxygen and forms a chemical bond. We have elected to use the known structure[12] of the phosphate anion PO_4^{3-} (tetrahedral symmetry, 1.54 Å bonds) as input data to aid in selection of a suitable ϕ_{PO}. The end result of such considerations (along with a desire for maximal simplicity) was the following function:

$$\phi_{PO}(r) = [43\,181.697\exp(-3.349r) - 3321.669]/r - 75\exp[-9(r-1.54)^2]\,, \tag{2.4}$$

wherein kcal/mol and angstroms, respectively, have been used for energy and distance units. This function exhibits a single minimum of depth -2172.67 kcal/mol at distance 1.297 Å. Stabilization of PO_4^{3-} at the greater bond length 1.54 Å reflects primarily the repulsions operating between the oxygens.

With the given interactions, the polarization model assigns the following potential energy to the phosphate anion at its mechanically stable minimum

$$\Phi[PO_4^{3-}] = -5005.39 \text{ kcal/mol}\,. \tag{2.5}$$

The convention used is that zero corresponds to widely separated and noninteracting particles.

III. MOLECULAR STRUCTURES

Having fixed ϕ_{PO}, the polarization model procedure specified in Appendix A then permits the potential energy Φ to be evaluated for any configuration of H^{+}, O^{2-}, and P^{5+} particles. Before proceeding to study condensed phases composed of these particles, it is important to see if the model is faithful to the known structural chemistry of pentavalent phosphorous. By construction, we have assured that PO_4^{3-} will possess the proper stable geometry. However, there are other key compounds that need to be checked.

The most natural starting point perhaps is the orthophosphoric acid molecule H_3PO_4. In order to seek the configuration of minimum potential energy for this species, we started with a PO_4^{3-} tetrahedral anion and three H^{+} particles at relatively large distances therefrom. All eight nuclei were then repeatedly displaced in sequence by small amounts, with only those displacements retained if Φ decreased. This "random" search procedure finally produced the structure illustrated in Fig. 1 after no further reduction in Φ seemed possible, even after displacement magnitudes had been halved several times.

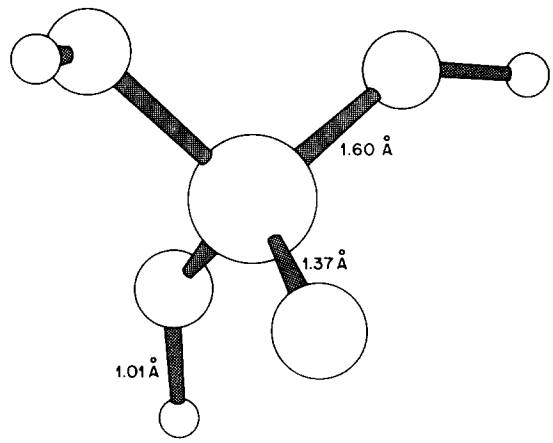

FIG. 1. Minimum energy structure for the orthophosphoric acid molecule H_3PO_4 according to the polarization model.

Not surprisingly, the result shows that the hydrogens attach to three of the four oxygen vertices of the phosphate tetrahedron, causing the latter to distort only to a modest extent. The structure shown appears to have a plane of symmetry. Note that none of the hydrogens form symmetrical bridges between pairs of oxygens. The energy of this orthophosphoric acid was computed to be

$$\Phi[H_3PO_4] = -6368.9 \text{ kcal/mol}\,. \tag{3.1}$$

Unfortunately, the gas phase molecular structure of H_3PO_4 has not been determined, probably because the substance is relatively involatile. However, the crystal structure has been determined, and seems fully consistent with the result shown in Fig. 1. Separate and distinct phosphate tetrahedra are observed in the crystal with P–O bonded distances 1.52 Å (once) and 1.57 Å (three times).[13] These are sufficiently close to our 1.37 and 1.60 Å, that the differences can be attributed partly to crystal forces, though doubtless the polarization model has some inherent error.

A similar computer search has been carried out to determine the stable structure for an isolated pyrophosphoric acid molecule $H_4P_2O_7$. This species results by splitting out a water molecule from a pair of orthophosphoric acid molecules. The result is displayed in Fig. 2. Two phosphate tetrahedra now share an oxygen vertex, and the four hydrogens are distributed two and two between the tetrahedra. The corresponding energy obtained in the calculation is

$$\Phi[H_4P_2O_7] = -11764.6 \text{ kcal/mol}\,. \tag{3.2}$$

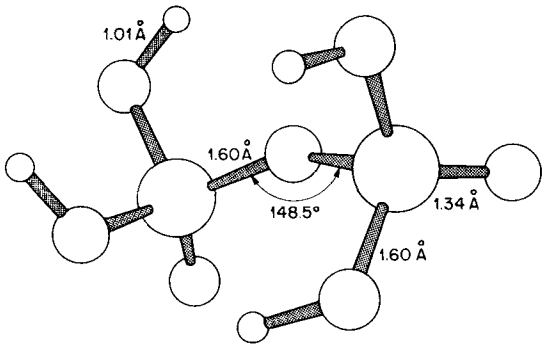

FIG. 2. Minimum energy structure for the pyrophosphoric acid molecule $H_4P_2O_7$ according to the polarization model.

A distinctive bend occurs at the shared vertex, with the P–O–P angle found to be 148.5°. The structure shown in Fig. 2 appears to have no symmetry.

Once again, no experimental gas-phase structure is available. Nevertheless, some indication of validity for Fig. 2 emerges from crystal structures of metal pyrophosphates. These materials consistently show $P_2O_7^{4-}$ units composed of vertex-sharing PO_4 tetrahedra with a substantial bend at the common oxygen. In the case of $Na_4P_2O_7 \cdot 10H_2O$, this bend angle is found to be 133.5°; the same study reveals P–O distances in the anion of 1.61 Å (bridge) and 1.51 Å (outer).[14] These stand in reasonably good agreement with the values indicated in Fig. 2.

The ability of the polarization model to produce bent P–O–P bonds at shared tetrahedral vertices is significant. Larger linear polyphosphates experimentally also exhibit this structural feature, as do cyclic polyphosphates, and the resulting stereochemistry is probably important in the ability of these substances to bind multivalent metal ions.[15]

The bent P–O–P bonding also appears in the minimum energy structure predicted for P_2O_5 by the present polarization model. Figure 3 gives the result of the configurational search over all atomic positions. The corresponding energy is

$$\Phi[P_2O_5] = -9636.2 \text{ kcal/mol} . \quad (3.3)$$

The reason underlying the P–O–P bending in the present polarization model context is the same as that which explains the nonlinearity of the water molecule.[1] In each case, a polarizable oxygen is flanked by two positive ions, P^{5+} in the phosphate case and H^+ for water. The dipole which is induced at the oxygen when the positive charges are *not* directly opposed interacts back with those charges (through Φ_{pol}) and stabilizes the nonlinear deformation.

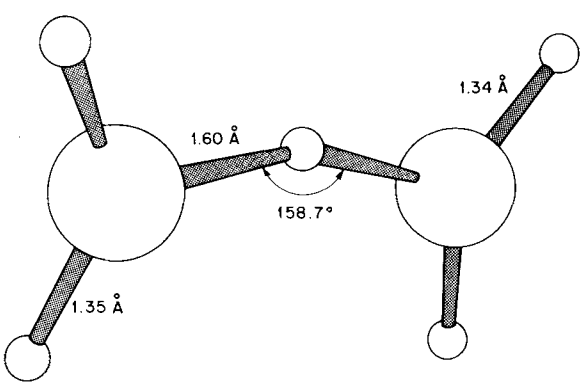

FIG. 3. Energy-optimized structure for P_2O_5 according to the polarization model.

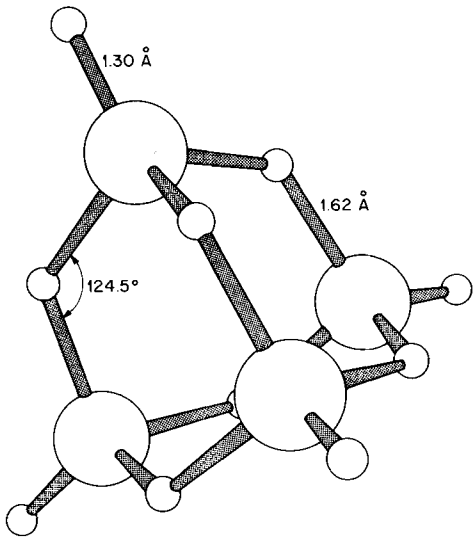

FIG. 4. Energy-optimized structure for P_4O_{10} according to the polarization model.

The P_2O_5 molecule is never observed as such in isolation. The reason is its strong tendency to dimerize to form the molecule P_4O_{10}. This latter species has been observed in a metastable crystal form[16] and its structure has been determined both in the crystal[17] (x-ray diffraction) and in the vapor phase[18] (electron diffraction). The result of the configurational search for the minimum energy structure within the polarization model is presented in Fig. 4; its energy was found to be

$$\Phi[P_4O_{10}] = -19445.9 \text{ kcal/mol} . \quad (3.4)$$

The predicted form has tetrahedral symmetry, with phosphorous vertices and bridging oxygens, in agreement with both crystal and vapor phase observations. The P–O bond lengths in Fig. 4 (1.62 Å for bridges, 1.30 Å for pendants) compare reasonably well with the electron diffraction results from Ref. 18 (1.62 Å for bridges, 1.39 Å for pendants). The P–O–P bond angle (124.5° in Fig. 4) also compares favorably with that reported in Ref. 18 (123.5°).

The evidence just presented indicates that the polarization model is at least qualitatively successful in representing the structural chemistry of penavalent phosphorous oxides and their related acids. On this basis, it seems justified to employ this model for statistical mechanical investigation of condensed phases formed out of these substances.

IV. MONTE CARLO PROCEDURE

We have employed the Monte Carlo method of computer simulation in order to examine implications of the po-

larization model for liquid phosphoric acid. Details of this technique, including the Metropolis sampling procedure that we used, have been adequately reviewed elsewhere.[19]

The specific system examined involved 27 phosphorous, 108 oxygen, and 81 hydrogen particles. They were confined to a unit cube with edge length 13.6338 Å; this size yields a mass density of 1.733 78 g/cm^3 to correspond to the experimental density of liquid H_3PO_4 extrapolated to 200 °C.[20]

Periodic boundary conditions apply at the six cube faces so that the perturbing influence of real surfaces or interfaces is eliminated. In order to account adequately for the long-range interactions between the charged and polarizable particles, we have employed a full Ewald summation as explained in Appendix B. No cutoffs have been invoked to simplify the computations.

While the given set of 216 particles can be assembled to form 27 distinct H_3PO_4 molecules, this is not the only chemical option. As explained below (Sec. VI), it is possible to select initial configurations for the system which predispose toward formation of condensed phosphates.

The many-body portion of the interaction Φ_{pol} in Eq. (2.1) is far and away the slower part of Φ to evaluate numerically. Therefore, we have found it expedient for any given starting configuration to begin the Monte Carlo relaxation toward equilibrium using *only* Φ_{pair}. Generating a Monte Carlo sequence of this stripped-down form quickly eliminates inadvertent overlaps and it also serves to establish nearly the correct chemical bond lengths. Furthermore, diffusive motions are enhanced by the quicker execution times so as to wipe away statistical memory of the initial configuration. Φ_{pol} must then be restored and the slower Monte Carlo sequence must be carried through a further relaxation period as proper bond angles establish themselves. Only after this second relaxation treatment is a Monte Carlo configuration sequence generated for the purpose of calculating thermodynamic properties and molecular distribution functions. Specific details are given in the following two sections.

After some experimentation, it was found that for the temperature used (200 °C), maximum steps for oxygen and phosphorous coordinates optimally should be set at ± 0.03 Å, while the corresponding limits for hydrogens should be ± 0.05 Å.

V. ORTHOPHOSPHORIC ACID

In order to assure the nominal presence of H_3PO_4 molecules, the 27 phosphorous particles were placed initially in a simple cubic array. Each was surrounded by four oxygens in a regular tetrahedral arrangement of fixed orientation at distance 1.54 Å. The initial positions of the 81 hydrogens were assigned by a random number generator, a feature that we felt would aid in subsequent randomization of PO_4^{3-} positions and orientations. This random placement had the effect of dislodging two of the oxygens from their tetrahedra; they were then reassigned new coordinates to restore the

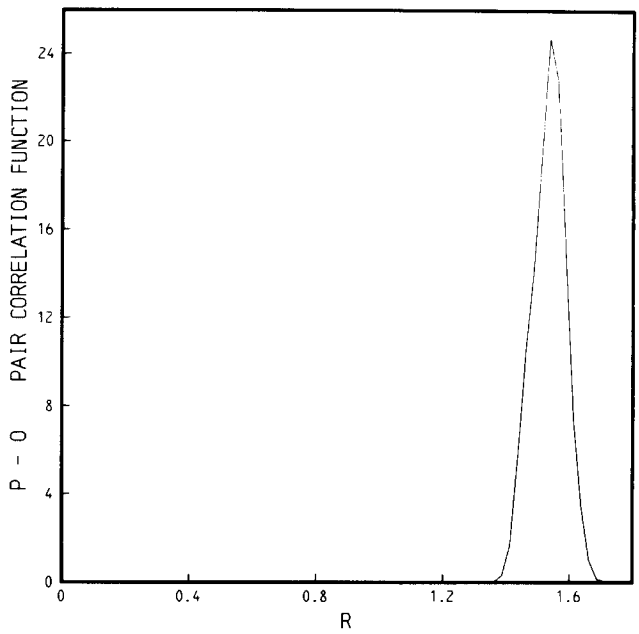

FIG. 5. Intramolecular part of the phosphorous–oxygen pair correlation function in orthophosphoric acid. The temperature is 200 °C. Distance units are angstroms.

PO_4^{3-} units. After this change had been effected, the system was run at 1000 °C, without Φ_{pol}, for 2016 full Monte Carlo cycles (each full cycle is a complete pass through the list of particle positions). This was followed by 2028 full cycles at 200 °C (still no Φ_{pol}), and then 1100 full cycles at 200 °C with the complete interaction Φ present. Only after this lengthy equilibration sequence was completed were averages computed, using 500 full cycles. From this last interval we find that the mean value of the potential energy for the 27-molecule system is

$$\langle \Phi \rangle = -171\,404.53 \text{ kcal/mol} . \qquad (5.1)$$

Figures 5–11 show pair correlation functions $g_{\alpha\beta}(r)$ for the various types of atom pairs α, β present in the system. Following the usual convention, these functions are normalized to unity at large r, where atomic occurrences are uncorrelated. Deviations of the $g_{\alpha\beta}$ from unity at small distances reveal details of statistical order. The distance unit for each of the figures is one angstrom.

The phosphorous-oxygen correlation function $g_{PO}(r)$ is shown in two parts, Figs. 5 and 6. The first shows the distances scale in the neighborhood of the P–O chemical bond length. The single isolated peak is produced by the phosphate tetrahedra present, with a breadth due to a combination of molecular vibrations and fluctuating intermolecular forces. The remainder of the correlation function is exhibited in Fig. 6, which reflects only intermolecular pairs. None of the latter is seen inside 3.0 Å; although noise is obviously present, there is evidently a peak centered around 3.7 Å that can be attributed to hydrogen-bonded pairs of neighboring H_3PO_4 molecules. Because of the small system size it would be misleading to carry the $g_{\alpha\beta}(r)$

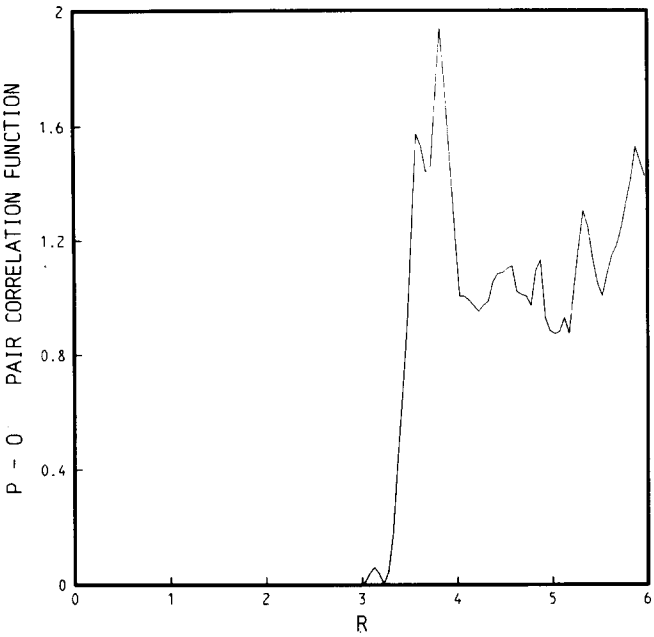

FIG. 6. Intermolecular part of the phosphorous–oxygen pair correlation function in orthophosphoric acid at 200°C.

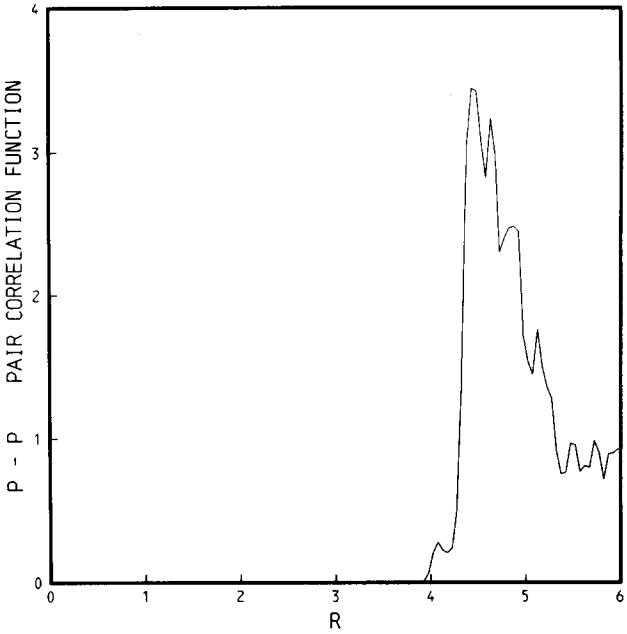

FIG. 8. Phosphorous–phosphorous pair correlation function in orthophosphoric acid at 200°C.

calculations beyond the 6 Å upper limit shown in Fig. 6. Nevertheless, a hint of a second broad maximum (at about 6 Å) appears to be present in Fig. 6.

Figure 7 presents the oxygen–oxygen pair correlation function. The tall and narrow maximum at about 2.5 Å obviously represents pairs of oxygens in the *same* PO_4 tetrahedron. But in contrast to the preceding P–O case, these intramolecular pairs are not fully resolved from the intermolecular pairs. Evidently, oxygens on neighboring tetrahedra can draw as close together as 2.5 Å either by having a short hydrogen bridge between them, or through approach to a triangular face by a vertex. Owing perhaps to the smoothing effect of rotations of tetrahedra, g_{OO} is rather featureless beyond about 3.3 Å.

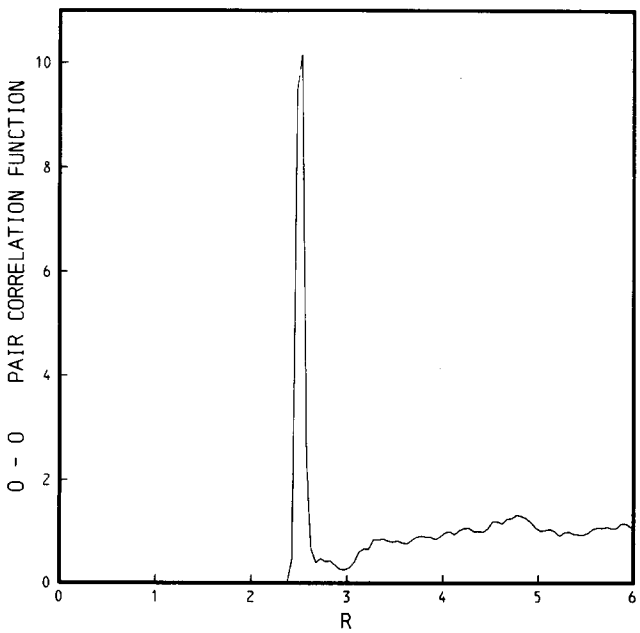

FIG. 7. Oxygen–oxygen pair correlation function in orthophosphoric acid at 200°C.

The prominent peak located at about 4.5 Å for g_{PP} (Fig. 8) clearly reveals nearest-neighbor PO_4 tetrahedra in the liquid. The fine structure shown is almost certainly spurious, and would be expected to disappear in a much longer Monte Carlo simulation. If it were possible as well to simulate a much larger phosphoric acid system, we would expect to find a broad second peak at approximately twice this first neighbor separation.

The hydrogen bonding structure in the liquid is revealed to some extent by the oxygen–hydrogen pair correlation function displayed in Fig. 9. The narrow grouping of closest pairs ($r \simeq 1.1$ Å) represents those which are covalently bonded. The next grouping which appears as a shoulder around 1.4 Å must represent hydrogen-bonding pairs which link neighboring PO_4 tetrahedra. The sum of these two distances 2.5 Å was mentioned above in connection with oxygen–oxygen correlation. Figure 9 also reveals the presence of a significant number of stretched "hydrogen bonds" up to approximately 2.2 Å in length.

We tentatively identify the g_{OH} maximum shown at 3.5 Å in Fig. 9 as stemming from pairs of PO_4 tetrahedra that are directly linked by a hydrogen bridge. But while it is the bridging hydrogen that is involved in that maximum, it must be paired with a pendant oxygen in either of the two tetrahedra, i.e., an oxygen not directly involved in the bridge.

Hydrogen bonding that links neighboring PO_4 units also shows up as structure in g_{PH}, Fig. 10. The double first peak arises from the asymmetric hydrogen bridges.

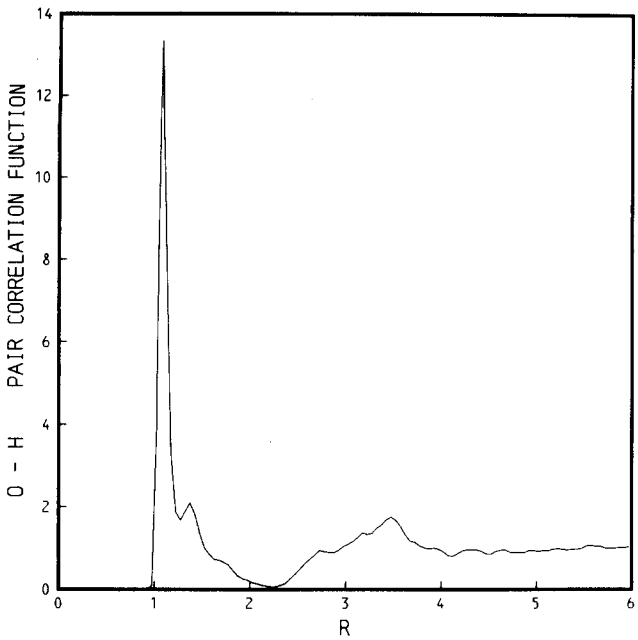

FIG. 9. Oxygen–hydrogen pair correlation function in orthophosphoric acid at 200°C.

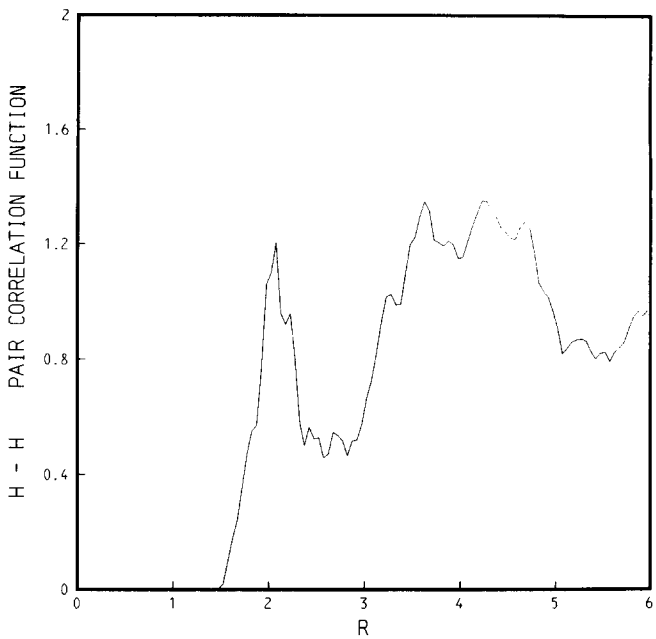

FIG. 11. Hydrogen–hydrogen pair correlation function in orthophosphoric acid at 200°C.

The component at smaller distance arises from P–H pairs covalently linked in the same HPO_4 unit, while the larger-distance component involves a PO_4 to which the H is hydrogen bonded.

Finally, Fig. 11 shows the distribution of H–H pairs. A major contribution to the first peak around 2.0 Å stems from pairs of H's near a given oxygen vertex, with one covalently bonded to the oxygen and the other hydrogen bonded to that oxygen.

In view of the acidity of the medium, gain or loss of hydrogens covalently attached to the PO_4 units has fundamental chemical interest. Information conveyed by the $g_{\alpha\beta}$ is not sufficient to characterize these hydrogen exchanges, however. Instead, it is necessary to monitor the distribution of hydrogen attachments to each of the PO_4 units. We have done this using the criterion that a hydrogen could only be considered "covalently bonded" to an oxygen provided their mutual separation were less than an upper cutoff radius

$$r_c = 1.30 \text{ Å} . \tag{5.2}$$

Even this criterion occasionally led to ambiguity, since a hydrogen could simultaneously be closer than r_c to two different oxygens (on distinct PO_4 units). In these cases, two possible conventions could be observed. (A) No more than one hydrogen is permitted (by definition) to be attached to any given oxygen, with shortest distances being identified first as "bonds" to eliminate ambiguities. (B) No maximum number of hydrogens bonded to any oxygen, but in the case of a bridging hydrogen simultaneously closer than r_c to two oxygens, it is assigned to the nearer of the two. Figure 12 indi-

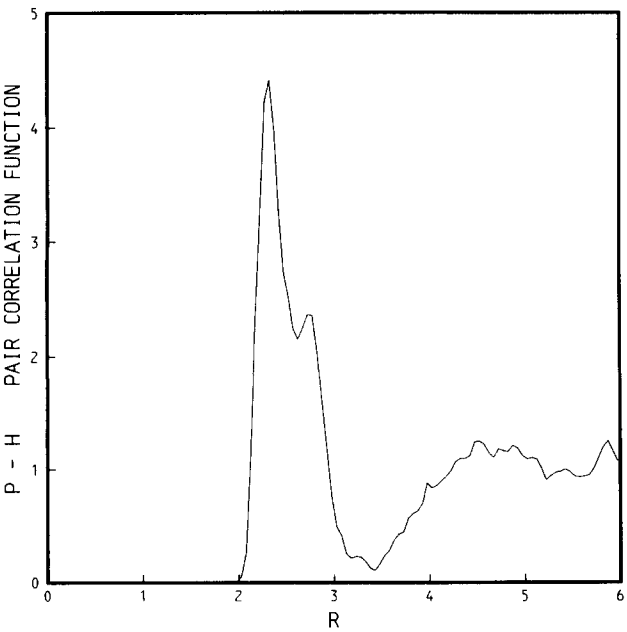

FIG. 10. Phosphorous–hydrogen pair correlation function in orthophosphoric acid at 200°C.

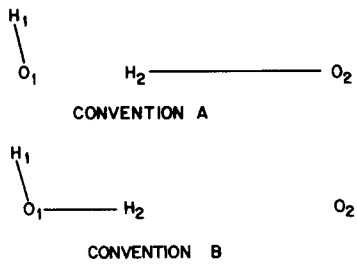

FIG. 12. Distinct conventions for assigning O–H "bonds." All three distances $r(O_1H_1) < r(O_1H_2) < r(O_2H_2)$ are less than r_c. Convention A limits the number of bonded H's to any O to a maximum of one; $r(O_1H_1)$ is first identified as a bond, leaving $r(O_2H_2)$ as the only other possible bond. With convention (B) (no maximum), the two shortest distances become bonds.

TABLE I. Assignment of hydrogens to PO_4 units in orthophosphoric acid at 200°C.

	Convention (A)			Convention (B)		
Step No.	$H_2PO_4^-$	H_3PO_4	$H_4PO_4^+$	$H_2PO_4^-$	H_3PO_4	$H_4PO_4^+$
500	8	11	8	8	11	8
600	5	17	5	5	17	5
700	5	17	5	5	17	5
800	8	14	5	6	15	6
900	7	14	6	6	15	6
1000	6	15	6	6	15	6

cates schematically how conventions (A) and (B) operate differently in assignment of H's to O's.

Table I shows how the hydrogens partition themselves among the 27 PO_4's at regular intervals during the Monte Carlo simulation. Data for both bonding conventions is exhibited, and in all cases, neutral H_3PO_4 molecules predominate. It is interesting to observe that when the two conventions differ (steps #800 and #900), Convention (B) accounts for all 81 H's in terms of the three species $H_2PO_4^-$, H_3PO_4, $H_4PO_4^+$, while the chemically more appealing Convention (A) leaves some H's totally unbonded. This observation shows that orthodox chemical intuition can be misleading or inappropriate for understanding local structure in complex liquids.

VI. POLYPHOSPHORIC ACID MIXTURE

In order to initiate simulation of the condensed phosphate-water mixture, the same 216 atoms (81 H's, 27 P's, 108 O's) were assigned random positions within the cubic unit cell with the same edge length as before 13.6338 Å. Our expectation was that as the Monte Carlo simulation proceeded, these atoms would sort themselves into a covalently bonded structure under influence of Φ, but that there was little chance for 27 disconnected PO_4 units to emerge. Instead, it was anticipated that some oxygen atoms would serve as shared vertices for PO_4 tetrahedra (as in $H_4P_2O_7$, Fig. 2), and for each such phosphate linkage, an excess water molecule would have to appear somewhere in the system. Subsequent events proved these expectations to be substantially correct.

Following the random initial placement of atoms, a Monte Carlo relaxation sequence, all at 200 °C, was implemented:

(a) 443 full cycles with only Φ_{pair} present;

(b) 108 full cycles with Φ_{pol} included to observe the effect of this term on execution time;

(c) 2420 full cycles again with only Φ_{pair} present;

(d) moving of one oxygen (which had remained unbound) to complete a nearby PO_4 unit;

(e) 720 full cycles with only Φ_{pair} present;

(f) 398 full cycles with both Φ_{pair} and Φ_{pol} present.

The Monte Carlo run used to calculate averages then followed, and consisted of 600 full cycles with the full polarization model potential present. The average value of the potential energy during this phase was found to be

$$\langle \Phi \rangle = -171\,807.02 \text{ kcal/mol} . \quad (6.1)$$

Figure 13 schematically indicates the polymerization pattern that formed during the preparation phase of the Monte Carlo simulation and that persisted throughout the final averaging phase. Since 17 shared oxygen vertices are present in the pattern shown, there are also 17 water molecules present in the system. Although cyclic oligomers could have formed in principle, and an infinite linear polymer would have been possible with the periodic boundary conditions, these options were avoided in the single system preparation used.

Figure 14 shows stereo views of the precise positions of the atoms at the end of the final averaging phase. Covalent P–O bonds are indicated by solid lines, and covalent O–H bonds by dashed lines. It is interesting to see in this view that the phosphate chains have a zigzag character, bending at each shared oxygen vertex, thereby bearing out chemical expectations. By viewing the figure even casually, it is obvious that the polyphosphoric acid mixture is structurally very complex.

Atomic pair correlation functions have been evaluated

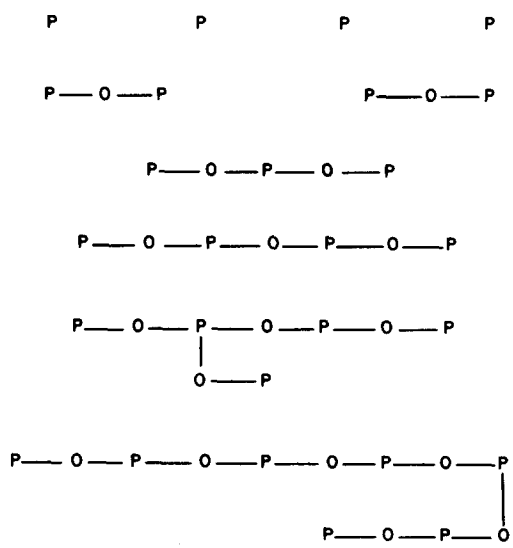

FIG. 13. Polymerization pattern present in the polyphosphoric acid mixture. Only shared oxygen vertices are shown for simplicity, though each phosphorous is actually surrounded by four oxygens. Seventeen water molecules also inhabit the system, one for each shared oxygen vertex.

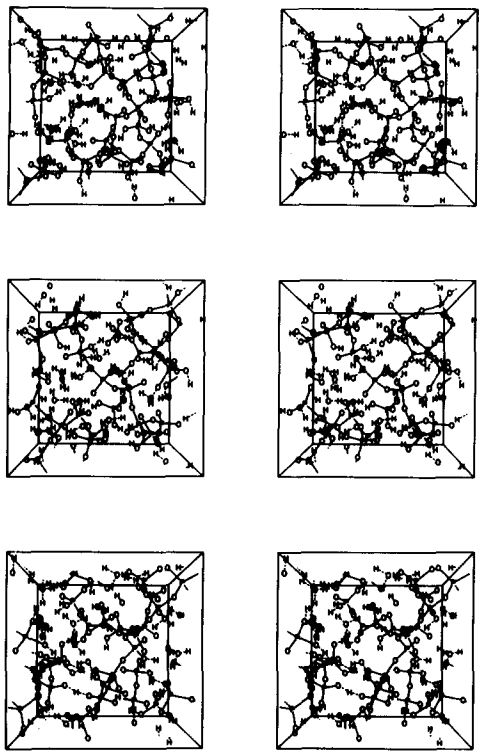

FIG. 14. Stereo pictures (along x, y, and z directions) of atomic positions at the end of the polyphosphoric acid mixture simulation.

for the mixture. Results are presented graphically in Figs. 15–21. Comparison with the respective Figs. 5–11 provides illuminating contrasts between the two liquids.

As was the case with orthophosphoric acid, the phosphorous–oxygen pairs fall into two separated groups.

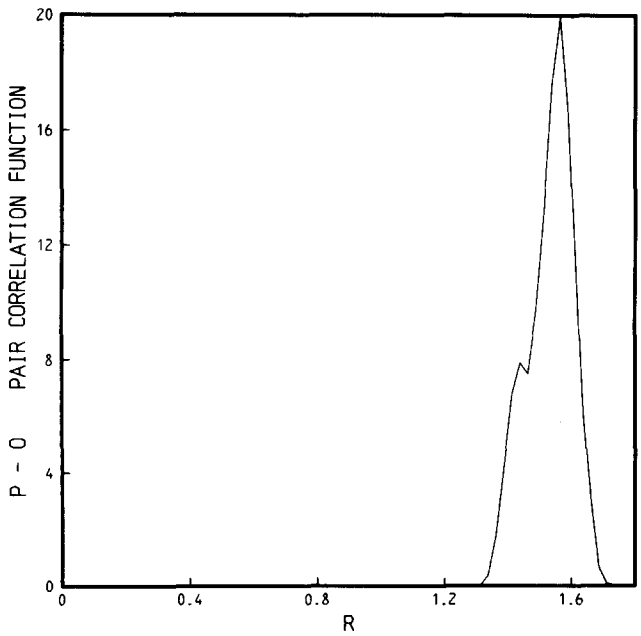

FIG. 15. Intramolecular part of the phosphorous–oxygen pair correlation function in the polyphosphoric acid mixture. The temperature is 200°C. Distance units are angstroms.

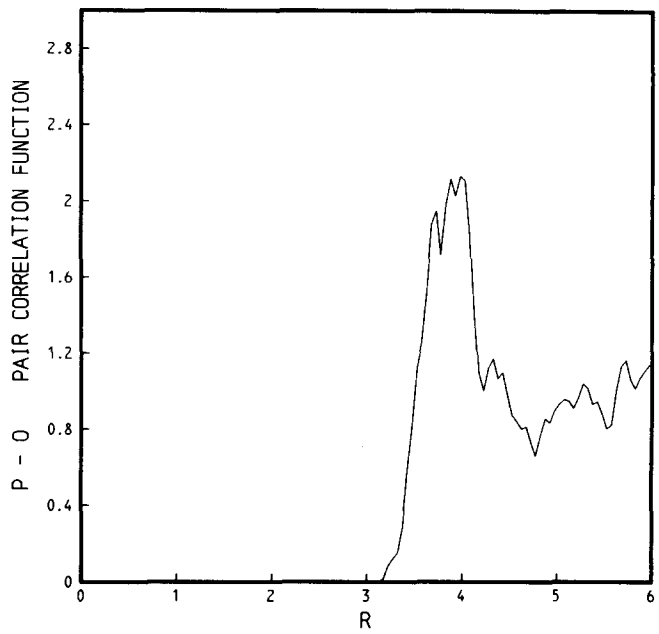

FIG. 16. Intermolecular part of the phosphorous–oxygen pair correlation function in the polyphosphoric acid mixture at 200°C.

Figure 15 presents the distribution of covalently bonded P–O pairs, which is somewhat broader than that shown earlier in Fig. 5. The extra breadth is due to the distorting effect on oxygen tetrahedra of vertex sharing. The nonbonded P–O pairs shown in Fig. 16 have a slightly better-developed first peak than before (Fig. 6), owing probably to rigid vertex linking of neighboring PO_4 units, one each of which contains the relevant P and O.

The oxygen–oxygen pair correlation function displayed in Fig. 17 still possesses a prominent first peak

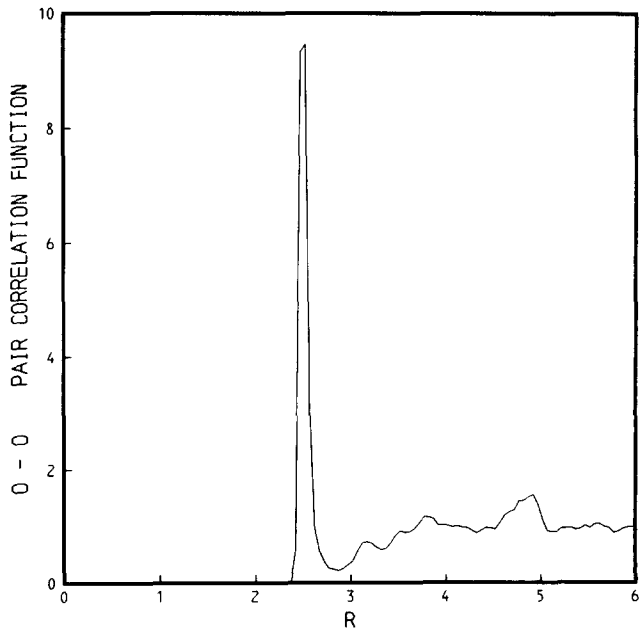

FIG. 17. Oxygen–oxygen pair correlation function in the polyphorphoric acid mixture at 200°C.

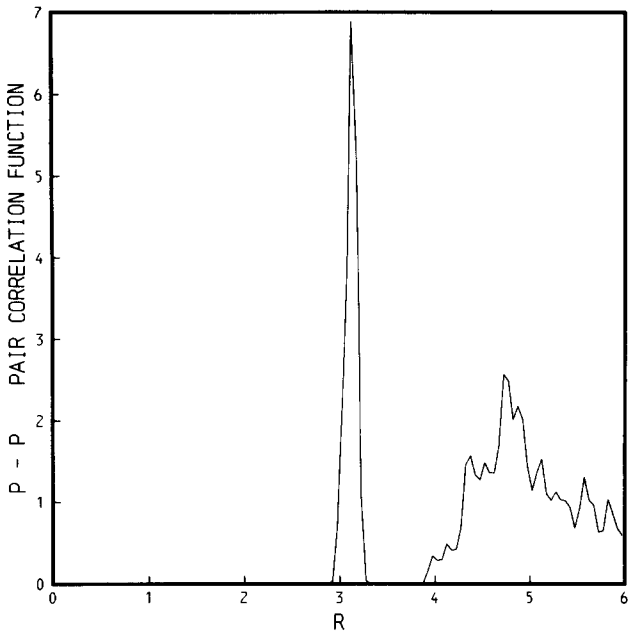

FIG. 18. Phosphorous–phosphorous pair correlation function in the polyphosphoric acid mixture at 200°C.

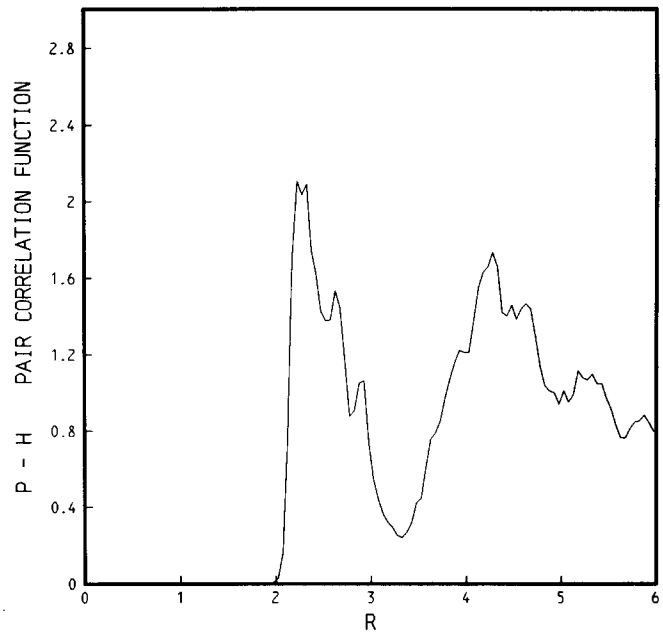

FIG. 20. Phosphorous–hydrogen pair correlation function in the polyphosphoric acid mixture at 200°C.

around 2.5 Å, arising from oxygens in the same PO_4 unit. The peak is slightly broadened and reduced in maximum magnitude due again to distortion of vertex sharing tetrahedra.

The structural difference between the orthophosphoric acid and the polyphosphoric acid mixture is most obvious when the corresponding g_{PP} functions are compared. The sharp and completely resolved peak near 3.1 Å in Fig. 18 has no analog in the preceding Fig. 8. This peak is obviously due to phosphorous pairs whose tetrahedra share an oxygen vertex. The narrowness of this peak shows how well defined the bond lengths and angles in this structural unit tend to be, even at 200 °C. The fact that the second peak in Fig. 18 is substantially reduced in comparison with its relative in Fig. 8 reflects the diminished volume element available when a zig-zag chain of linked phosphate units threads its way through an origin centered on one of its backbone P's. The presence of that chain permits fewer nonbonded PO_4 units to exist as close neighbors to the origin P.

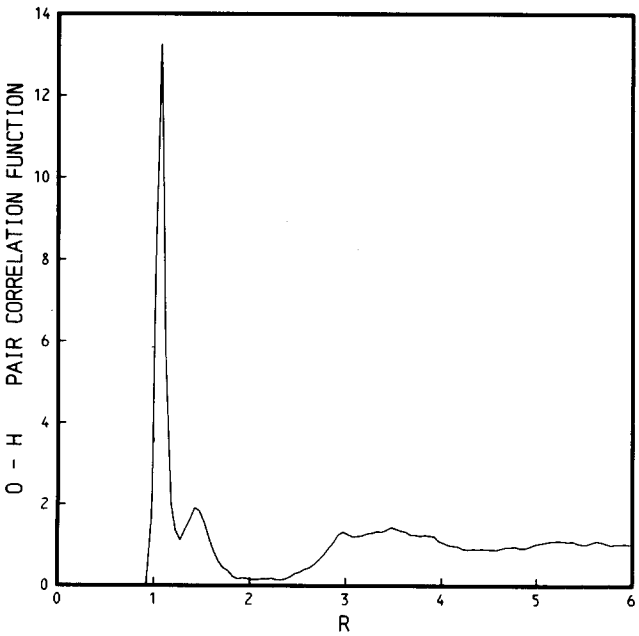

FIG. 19. Oxygen–hydrogen pair correlation function in the polyphosphoric acid mixture at 200°C.

The oxygen–hydrogen pair correlation function shown in Fig. 19 superficially appears to be quite similar to its monomeric analog in Fig. 9. The sharp first peaks are virtually identical, as might be anticipated from the assumption that every hydrogen is bonded somewhere in each system to an oxygen. The hydrogen-bonding second maximum appears to be a bit better developed in this polymeric case, though the distinction is probably at the margin of statistical significance. Finally, the third obvious maximum at 3.5 Å in Fig. 9 seems to be substantially broadened in Fig. 19, probably as a result of molecular heterogeneity. There is no direct information present in either g_{OH} result which directly indicates acidity of the media.

The reduction in the first g_{PH} peak in passing from Fig. 10 (orthophosphoric) to Fig. 20 (polyphosphoric) can be explained by the fact that the latter system can transfer protons from PO_4 units to the 17 ambient water molecules. In the orthophosphoric acid, this process is not available and, on the average, 3 H's will be bonded [at least in convention (B)] to each PO_4 at an average distance of about 2.3 Å from the central phosphorous. But now some of the hydrogens have simply migrated by acid dissociation followed by reattachment to the more basic water molecules. In fact, careful examination of Fig. 14 and other system con-

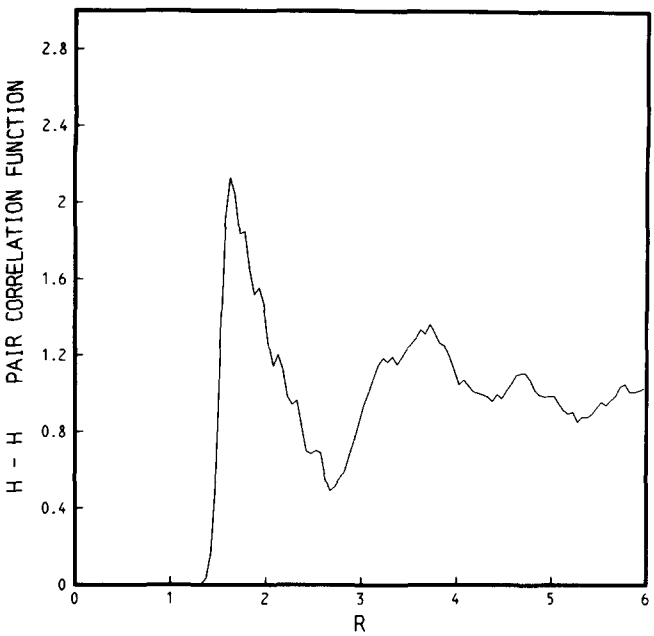

FIG. 21. Hydrogen–hydrogen pair correlation function in the polyphosphoric acid mixture at 200°C.

figuration pictures we have produced shows the presence of H_3O^+ and $H_5O_2^+$ ions in the mixture that result from this acid dissociation and proton transfer process.

Finally, we note that the strong enhancement in the first peak of g_{HH} that results from the orthophosphoric to polyphosphoric transformation can also be explained by the presence of water and by acid dissociation. In the water molecules themselves, as well as in the proton hydrates, H–H distances in the range 1.5–1.8 Å occur in the known molecular structures and, evidently, show up in Fig. 21 in that distance range.

Three types of oxygen atoms can be distinguished in the polyphosphoric acid mixture. They are (1) bridging oxygens (shared vertices), (2) peripheral oxygens (those in PO_4 units that are *not* shared vertices), and (3) water oxygens. Using convention (B) and the same r_c as before (1.30 Å) we monitored the bonding statistics of hydrogens to each of these types of oxygens during a portion of the simulation. The results obtained were as follows:

$$\begin{aligned} &\text{H's/bridging O} = 0.000\ , \\ &\text{H's/peripheral O} = 0.590\ , \\ &\text{H's/water O} = 2.449\ . \end{aligned} \tag{6.2}$$

Evidently, the bridging oxygens are the least basic of the three types, a result which seems not to have been suggested before. The fact that the water oxygens on average bear more than their usual complement of two hydrogens indicates (consistent with above remarks) that the polyphosphoric acid is indeed acting as an acid and transferring protons to the more basic water. On the basis of the last of the three numbers in Eq. (6.2) and recalling that there are 17 water molecules present, one easily calculates that the solvated hydrogen ion concentration is 5.0 mol/liter.

VII. CONCLUSION

We believe the major value of the project reported here is that it establishes the feasibility of simulating phosphoric acid media at the molecular level. Our work needs to be extended in several directions. The most obvious is that longer simulation runs are required to reduce statistical errors and it is clearly desirable to use larger systems than that employed here. In the case of polyphosphoric acid mixtures, it would be valuable to generate several random initial configurations to see if the resulting polymerization patterns differ widely and if the corresponding averaged properties likewise scatter.

The prospects for future applications are diverse and exciting, even though substantial computing power will be required. We have demonstrated, by example, that hydrogen ion concentrations can be determined in the highly acidic and complex polyphosphoric acid mixture; it is desirable to make a series of such determinations at different temperatures, water contents, and degrees of phosphate polymerization. No insuperable difficulties should arise in changing boundary conditions from threefold periodicity, used in the present work, to boundary conditions appropriate for matter contained between charged and conducting boundaries; this would permit the study of double layer structure for phosphoric acid–electrode interfaces. In addition to these Monte Carlo studies of static molecular structure, it should also be possible to study kinetic features using the molecular dynamics method.[3,21]

At the most fundamental level, the various input functions used in the polarization model should be re-examined. Doubtless, some improvements could be effected, though for phosphorous-containing compounds such as those in Figs. 1–3, it may first be necessary to determine precise energies and geometries by experiment and/or accurate quantum mechanical calculations. The polarization model can also be extended chemically to include other inorganic ions (e.g., K^+, Ca^{2+}, NH_4^+, Cl^-, SO_4^{2-}) so that a wide variety of phosphate solutions could be examined. The final product of these efforts would be a powerful tool to aid in understanding many of the complex liquids that are important in chemistry and chemical technology.

APPENDIX A

The distinct atomic species considered by the polarization model are assigned fixed charges or oxidation states (q_i) and fixed scalar polarizabilities (α_i). The value 1.444 Å^3 is used for polarizability of the O^{2-} particles, while H^+ and P^{5+} are assumed to have vanishing polarizabilities.

The first component of the total potential energy Φ, namely Φ_{pair}, has the following simple form:

$$\Phi_{\text{pair}} = \sum_{i<j} \phi_{ij}(r_{ij})\ . \tag{A1}$$

This summation includes a term for each pair of particles present in the system. There is one pair function ϕ_{ij} for every distinct pair of species ij present in

the system. It is partly the role of these ϕ_{ij} to describe charge–charge interactions at long range, so that

$$\phi_{ij} \sim q_i q_j / r_{ij} \quad (r_{ij} \to \infty) . \tag{A2}$$

It is also their role at short range to describe chemical bonding (if any) and overlap repulsion between atomic electron coulds.

As a result of the charges present in a collection of particles, dipoles μ_l will be induced on those particles. Except for one generalization, these dipoles will be determined by the same set of coupled linear equations familiar from classical electrostatics

$$O = \mu_l + \alpha_l \sum_{j(\neq l)} \frac{\mathbf{r}_{lj} q_j}{r_{lj}^3} [1 - K_l(r_{lj})] + \alpha_l \sum_{m(\neq l)} \frac{\mathbf{T}_{lm} \cdot \mu_m}{r_{lm}^3} [1 - K_l(r_{lm})] , \tag{A3}$$

where

$$\mathbf{T}_{lm} = 1 - \frac{3\mathbf{r}_{lm}\mathbf{r}_{lm}}{r_{lm}^2} . \tag{A4}$$

The generalization involves the factors $1 - K_l$ which are identically unity in classical electrostatics. As a result of spatial extension for atomic electron clouds we permit these factors to deviate from unity at distances comparable to atomic sizes. In particular for every polarizable species l the factor $1 - K_l$ must vanish at least cubically at the origin.[1]

The second component of Φ, $\Phi_{\rm pol}$, is a bilinear form in charges and dipole moments:

$$\Phi_{\rm pol} = \frac{1}{2} \sum_{\substack{i,l \\ (i \neq l)}} \frac{(\mu_l \cdot \mathbf{r}_{li}) q_i}{r_{li}^3} [1 - L_l(r_{li})] . \tag{A5}$$

Once again, this has the form appropriate to classical electrostatics of point particles, except for correction factors $1 - L_l$ that account for spatial extension of electron clouds and that vanish cubically at the origin.

Using kcal/mol and angstroms respectively for energy and distance units, the central pair potentials required for the phosphoric acid simulation are as follows ($r_e = 0.9584$):

$$\phi_{\rm HH} = 332.1669/r , \tag{A6}$$

$$\phi_{\rm OO} = 1328.6676/r + 8.255 \exp[-18.665(r - 2.45)] + \frac{84.293}{1 + \exp[2.778(r - 2.56)]} - \frac{12.299}{1 + \exp[4.817(r - 3.10)]} , \tag{A7}$$

$$\phi_{\rm PP} = 8304.1725/r , \tag{A8}$$

$$\phi_{\rm OH} = [3321.669 \exp(-3.699\,392\,82r) - 664.3338]/r + [-184.696\,674\,3(r - r_e) + 123.976\,218\,8(r - r_e)^2] \times \exp[-16(r - r_e)^2] ; \tag{A9}$$

$$\phi_{\rm PH} = 1660.8345/r ; \tag{A10}$$

$$\phi_{\rm PO} = [43181.697 \exp(-3.349r) - 3321.669]/r - 75 \exp[-9(r - 1.54)^2] . \tag{A11}$$

Because H^+ and P^{5+} have both been treated as unpolarizable, factors $1 - K$ and $1 - L$ are required only for the species O^{2-}. The specific functions employed in the present simulation study are

$$1 - K_O = r^3/[r^3 + F(r)] , \quad F(r) = 1.855\,785\,223(r - r_e)^2 \times \exp[-8(r - r_e)^2] + 16.951\,457\,27 \exp(-2.702\,563\,425r) ; \tag{A12}$$

$$1 - L_O = 1 - \exp(-3.169\,888\,166r)[1 + 3.169\,888\,166r + 5.024\,095\,492r^2 - 17.995\,990\,78r^3 + 23.922\,85r^4] . \tag{A13}$$

APPENDIX B

Polarization model details presented in the preceding Appendix A relate to evaluation of the potential energy Φ for any isolated group of particles. However, the use of periodic boundary conditions in our statistical mechanical simulation, chosen as usual to eliminate unwanted surface effects, necessitates a basic modification. On account of the long-range nature of electrostatic interactions, it becomes obligatory to sum over infinite periodic arrays of field sources. It is the purpose of this appendix to supply a convenient (if only approximate) algorithm for carrying out such sums in closed form.

We base our considerations on the solution $M(r)$ to the Poisson equation, in the unit cube, appropriate to a unit point charge at its center and a uniform neutralizing negative background charge

$$\nabla^2 M(\mathbf{r}) = 4\pi[1 - \delta(\mathbf{r})] . \tag{B1}$$

We seek that solution which is periodic throughout all space, so we require that the gradient of M vanish on the surface of the unit cube. The solution will have a simple pole at the origin (due to the unit charge) and at each of the periodic images of the origin. Without the negative background, a periodic solution would not exist.

We propose to use a suitably scaled version of M as a replacement for the Coulombic pair interaction, when periodic replication is involved. Specifically, let us consider the case of N point charges $q_1 \cdots q_N$ at positions $\mathbf{r}_1 \cdots \mathbf{r}_N$. As is the case in our Monte Carlo simulation, we shall suppose that the net charge vanishes,

$$\sum_{i=1}^{n} q_i = 0 . \tag{B2}$$

The conventional charge–charge interaction for this collection of particles in isolation is

$$\sum_{i<j=1}^{n} q_i q_j / r_{ij} , \tag{B3}$$

but, if instead, the collection is housed in a primitive cubic cell with edge Γ to which periodic boundary conditions apply, we replace expression (B3) by

$$\sum_{i<j=1}^{n} (q_i q_j / \Gamma) M(\mathbf{r}_{ij}/\Gamma) . \tag{B4}$$

Note that expression (B4) has the proper divergence when particle i approaches particle j or any of its infinite number of images. On account of the electroneutrality

condition (B2), the uniform background charge for all particles taken together vanishes identically.

On account of the periodicity of M, the dipole moment of the n-charge collection, which is replicated in each image of the Γ^3 cell, cannot give rise to reaction fields that normally are associated with surface charges. The appropriate physical interpretation to be invoked for our use of M is that the primitive cell, embedded in a large set of its images, constitutes a supersystem which is surrounded by an electrical conductor. This conductor serves to cancel surface charges and thereby eliminate reaction fields. At the same time the primitive cell is so deeply buried in its images that distortions of electrical fields near the conductor-surface image interface never penetrate to that primitive cell.

If each of the pair potentials ϕ_{ij} discussed in Appendix A is written in the form

$$\phi_{ij}(r) = f_{ij}(r) + q_i q_j / r \,, \tag{B5}$$

then the function f_{ij} isolates the short-range non-Coulombic contributions. For the cube edge Γ used in our simulation, it is unnecessary to include f's from images in computing potential energies since the contributions die away sufficiently rapidly, with increasing distance. Hence, with periodic boundary conditions, we simply modify Eq. (B5) to

$$\phi_{ij}(\mathbf{r}) = f_{ij}(r) + (q_i q_j / \Gamma)\, M(\mathbf{r}/\Gamma) \,. \tag{B6}$$

Analogous modifications apply to the calculation of induced dipole moments on the polarizable particles in the polarization model and to evaluation of the many-body polarization interaction. Firstly, the linear equations (A3) for self-consistent determination of the induced moments in the isolated system are modified to the following form with periodic boundary conditions

$$0 = \boldsymbol{\mu}_l + \alpha_l \sum_{j(\neq l)} \left\{ \frac{\mathbf{r}_{lj} q_j}{r_{lj}^3} [1 - K_l(r_{lj})] + \nabla_{lj} \left[\frac{q_j}{r_{lj}} - \frac{q_j}{\Gamma} M\left(\frac{\mathbf{r}_{lj}}{\Gamma}\right) \right] \right\} + \alpha_l \sum_{m(\neq l)} \left\{ \frac{\mathbf{T}_{lm}}{r_{lm}^3} [1 - K_l(r_{lm})] + \nabla_{lm} \nabla_{lm} \left[\frac{1}{r_{lm}} - \frac{1}{\Gamma} M\left(\frac{\mathbf{r}_{lm}}{\Gamma}\right) \right] \right\} \cdot \boldsymbol{\mu}_m \,. \tag{B7}$$

[Here we have recognized that the K_l (like the f's above) are sufficiently short ranged to neglect for images.] Secondly, the polarization potential [Eq. (A5)] must be modified to

$$\Phi_{\text{pol}} = \frac{1}{2} \sum_{\substack{i,l \\ (i \neq l)}} \boldsymbol{\mu}_l \cdot \left\{ \frac{q_i \mathbf{r}_{li}}{r_{li}^3} [1 - L_l(r_{li})] + \nabla_{li} \left[\frac{q_i}{r_{li}} - \frac{q_i}{\Gamma} M\left(\frac{\mathbf{r}_{li}}{\Gamma}\right) \right] \right\} . \tag{B8}$$

We are now left with the task of constructing a useful approximation for the function M. Consider first the following auxiliary function:

$$F(\mathbf{r}) = 1/(2\pi)^2 \{ \tfrac{49}{6} - 3[\cos(2\pi x) + \cos(2\pi y) + \cos(2\pi z)] + \tfrac{3}{10}[\cos(4\pi x) + \cos(4\pi y) + \cos(4\pi z)] - \tfrac{1}{15}[\cos(6\pi x) + \cos(6\pi y) + \cos(6\pi z)] \} = r^2 \left\{ 1 - \frac{(2\pi)^6}{560} \left(\frac{x^6 + y^6 + z^6}{r^2} \right) + \cdots \right\} . \tag{B9}$$

Because it is periodic, F will vanish as shown at the origin and at each unit-cell image of the origin (i.e., the simple cubic lattice with unit spacing). Next, we write

$$M(\mathbf{r}) = [F(\mathbf{r})]^{-1/2} + G(\mathbf{r}) \,. \tag{B10}$$

The first term on the right yields the required set of simple poles on the simple cubic lattice. G is incorporated to make M satisfy the Poisson equation (B1), but it is bounded. Like M and F, G is periodic and so it is natural to expand this function as a Fourier series. Owing to condition (B2), we have the freedom to select an arbitrary additive constant in G without affecting the potential energy, and thus we can require

$$G(0) = 0 \,. \tag{B11}$$

The expression finally selected for G is

$$\begin{aligned} G(\mathbf{r}) \simeq\ & G_0 + G_1 [\cos(2\pi x) + \cos(2\pi y) + \cos(2\pi z)] \\ & + G_2 [\cos(2\pi x)\cos(2\pi y) + \cos(2\pi x)\cos(2\pi z) \\ & + \cos(2\pi y)\cos(2\pi z)] + G_3 \cos(2\pi x)\cos(2\pi y) \\ & \times \cos(2\pi z) + G_4 [\cos(4\pi x) + \cos(4\pi y) + \cos(4\pi z)] \\ & + G_5 [\cos(4\pi x)\cos(2\pi y) + \cos(2\pi x)\cos(4\pi y) \\ & + \cos(4\pi x)\cos(2\pi z) + \cos(2\pi x)\cos(4\pi z) \\ & + \cos(4\pi y)\cos(2\pi z) + \cos(2\pi y)\cos(4\pi z)] \,. \end{aligned} \tag{B12}$$

The six coefficients $G_0 \cdots G_5$ were determined by Eq. (B11); by requiring that the Poisson equation (B1) be satisfied at the points in and on the unit cube

$$(0, 0, 0) \,, \quad (\tfrac{1}{2}, 0, 0) \,, \quad (\tfrac{1}{2}, \tfrac{1}{2}, 0) \,, \quad (\tfrac{1}{2}, \tfrac{1}{2}, \tfrac{1}{2}) \,; \tag{B13}$$

and by imposing the correct Madelung energy for the CsCl structure[22] at spacing $3^{1/2}/2$

$$M(\tfrac{1}{2}, \tfrac{1}{2}, \tfrac{1}{2}) = 2.035\,356 \,. \tag{B14}$$

The resulting set of coefficients for Eq. (B12) is numerically found to be

$$\begin{aligned} G_0 &= 0.297\,600\,993\,8, & G_1 &= -9.935\,609\,384 \times 10^{-2}, \\ G_2 &= -3.485\,829\,184 \times 10^{-3}, & G_3 &= 3.058\,456\,248 \times 10^{-2}, \\ G_4 &= -2.406\,206\,406 \times 10^{-3}, & G_5 &= -2.073\,528\,006 \times 10^{-3} \,. \end{aligned} \tag{B15}$$

The accuracy of our closed-form approximation to $M(r)$ can be tested by using it to calculate the Madelung energy of the NaCl lattice at half the spacing used for condition (B14), namely, $3^{1/2}/4$

$$\tfrac{1}{2}[-3M(\tfrac{1}{2}, 0, 0) + 3M(\tfrac{1}{2}, \tfrac{1}{2}, 0) - M(\tfrac{1}{2}, \tfrac{1}{2}, \tfrac{1}{2})] = -1.738\,214\,462 \,. \tag{B16}$$

The exact value[22] is $-1.747\,564$, indicating an error of 0.54%. Note that regardless of the structure involved, use of our approximate $M(r)$ should entail less and less error as the density of ions increases in the basic cubic

cell. It is obvious that the precision of this method could be improved by including more Fourier components in the expansion for G, and by requiring simultaneously that the Poisson equation be satisfied on a denser grid.

[1]F. H. Stillinger and C. W. David, J. Chem. Phys. **69**, 1473 (1978).
[2]F. H. Stillinger, Int. J. Quantum Chem. **14**, 649 (1978).
[3]F. H. Stillinger, J. Chem. Phys. **71**, 1647 (1979).
[4]C. W. David, Chem. Phys. **40**, 229 (1979).
[5]F. H. Stillinger and C. W. David, J. Chem. Phys. **73**, 3384 (1980).
[6]C. W. David, Chem. Phys. **53**, 105 (1980).
[7]P. J. Turner and C. W. David, J. Chem. Phys. **74**, 512 (1981).
[8]S. J. Kiehl and E. Claussen, J. Am. Chem. Soc. **57**, 2284 (1935).
[9]L. F. Fieser and M. Fieser, *Reagents for Organic Synthesis* (Wiley, New York, 1967), Vol. 1, pp. 894–905.
[10]R. Noyes, *Fuel Cells for Public Utility and Industrial Power* (Noyes Data Corp., Park Ridge, New Jersey, 1977), p. 155.
[11]T. G. Spiro, in *Inorganic Biochemistry* (Elsevier, New York, 1973), Vol. 1, p. 549.
[12]L. Pauling, *The Nature of the Chemical Bond*, 3rd ed. (Cornell University, Ithaca, 1960), p. 321.
[13]*Gmelins Handbuch der Anorganischen Chemie, Achte Auflage. Phosphor, Teil C*, edited by A. Kotowski (Chemie-GMBH, Weinheim, 1965), p. 162.
[14]D. W. J. Cruickshank, Acta Crystallogr. **17**, 672 (1964).
[15]S. Greenfield and M. Clift, *Analytical Chemistry of the Condensed Phosphates* (Pergamon, New York, 1975), pp. 32–33.
[16]H. C. J. de Decker and C. H. MacGillavry, Recl. Trav. Chim. Pays-Bas **60**, 153 (1941).
[17]D. W. J. Cruickshank, Acta Crystallogr. **17**, 677 (1964).
[18]G. C. Hamson and A. J. Stosick, J. Am. Chem. Soc. **60**, 1814 (1938).
[19]J. P. Valleau and S. G. Whittington, in *Statistical Mechanics Part A: Equilibrium Techniques*, edited by B. J. Berne (Plenum, New York, 1977), pp. 137, 169.
[20]N. N. Greenwood and A. Thompson, J. Chem. Soc. **1959**, 3485.
[21]F. H. Stillinger and T. A. Weber, Chem. Phys. Lett. **79**, 259 (1981).
[22]R. Kubo and T. Nagamiya, *Solid State Physics* (McGraw–Hill, New York, 1968), pp. 16–17.